Supporting Information

Synergetic Effect of a Well-Defined Au@Pt Core-Shell Nanostructure toward Photocatalytic Hydrogen Generation: Interface Engineering to Improve Schottky Barrier and Hydrogen-Evolved Kinetics

Sung-Fu Hung,[a,†]Ya-Chu Yu,[a,†]Nian-Tzu Suen,[a] Guan-QuanTzeng,[a]Ching-Wei Tung,[a] Ying-YaHsu,[a,b] Chia-ShuoHsu,[a] Chung-Kai Chang,[c] Ting-Shan Chan,[c] Hwo-ShuennSheu,[c] Jyh-Fu Lee,[c] Hao Ming Chen[a,]*

[a]Department of Chemistry, National Taiwan University, Taipei 106, Taiwan.

[b]Program for Science and Technology of Accelerator Light Source, National Chiao Tung University, Hsinchu 300, Taiwan.

[c]National Synchrotron Radiation Research Center, Hsinchu 300, Taiwan.

Experimental Section

S1. Preparation of TiO_2 nanotubes

Cleaned Ti sheet was immersed into solution of HF-HNO_3-H_2O with volume ratio of 1:4:5 for 60 s to remove oxide on the surface of Ti sheet, and followed by washing with water and dried by N_2 stream. Electrochemical anodization was conducted at 60 V for 15 h at 20 °C, in which Ti sheet acted as the working electrode and Pt foil as the counter electrode. The electrolyte was prepared by

dissolving 1.7 g of NH_4F in 10 mL of DI water and followed by adding 500 mL of ethylene glycol. After the anodization, the as-prepared TiO_2 nanotubes were rinsed by DI water and dried by N_2 stream and then annealed at 450 °C for 3 h to increase the crystallinity.[21] To conduct further surface modification, TiO_2 nanotubes were scraping off from the Ti sheet.

S2. Synthesis of Au-Pt core-shell nanostructure

Au-Pt core-shell nanostructures (Au@Pt) were synthesized by chemically reducing a mixture of noble metal salts.[1] 6 mL of 0.1 M L(+)-ascorbic acid was added into the mixture of 3 mL of 20 mM chloroplatinic acid, 3mL of 20 mM chloroauric acid, and 0.06 g of Pluronic F-127 to reduce the metal salts to metal nanoparticles. After sonicating for 15 mins, the mixture was left undisturbed for 6 hours for formation of Au@Pt nanostructure. Au@Pt nanostructure was isolated by centrifugation at 10000 rpm for 20 mins, then removed the supernatant and dried at 50 °C.

S3. Self-assembling of TiO_2 NTs-Au@Pt composite

To achieve the self-assembling of TiO_2 NTs-Au@Pt composite, 4 mg of TiO_2 NTs and 4 mg of Au@Pt nanostructure were added into 20% 3-mercaptopropionic acid aqueous solution and stirred for 24 hours. The resulting TiO_2 NTs-Au@Pt nanostructure was isolated by centrifugation at 8000 rpm for 20 mins, then removed the supernatant and dried at 45 °C.

S4. Synthesis of TiO_2 NTs-AuPt random alloy

In order to synthesize the AuPt random alloy with the ratio of 0.25 Pt/Au , which was similar with the composition of Au@Pt, 17.3 μmol of $HAuCl_{4(aq)}$ and 5.8 μmol of $HPtCl_{6(aq)}$ were mixed with 10 mg of TiO_2 NTs in 10 mL DI water and stirred for 1.5 hours in the ice bath. Subsequently, 30 μmol of ice-cold $NaBH_4$ was added into the mixture and stirred for 3 hours in the ice bath. The resulting TiO_2 NTs-AuPt random alloy was isolated by centrifugation at 8000 rpm for 20 mins, then removed the supernatant and dried at 45 °C.

S5. Characterization

The morphologies of the photoelectrodes were characterized with field-emission scanning electron microscopy (FE-SEM, JEOL JSM-7600F), energy dispersive X-ray spectroscopy (EDS), and transmission electron microscopy (TEM, JEOL JEM-2100F). Absorption spectra were collected from a diffuse reflectance UV-Vis spectrophotometer equipped with an integrating sphere (JASCO, V-670). X-ray photoelectron spectroscopy (XPS) measurements were conducted on an ESCALAB250 photoelectron spectrometer (Thermo Fisher Scientific) at 2.4×10^{-10} torr using a monochromatic Al K_α X-ray beam (1486.60 eV). All binding energies (BEs) of the elements were calibrated to adventitious carbon at 284.50 eV. X-ray absorption spectra of gold and platinum L-edge were measured in X-ray transmission mode at room temperature using BL-17C and X-ray absorption spectra of titaninum L-edge were measured in total electron yield at room temperature using BL-20A at National Synchrotron Radiation Research Center

(NSRRC, Hsinchu, Taiwan) in which the electron storage ring was operating at 1.5 GeV with a beam current of 300 mA.

S6. Measurement of photocatalytic activity for hydrogen production

A homemade airtight cell was used to measure the evolution of hydrogen gas of the photocatalyst in the electrolyte composed of 0.5 M Na_2SO_4 and methanol with volume ratio of 4:1. 5 mg of total catalyst weight was added in the cell in each measurement. Argon bubbling purged the electrolyte in the cell under stirring for 30 mins to remove any dissolved oxygen before the measurement of the hydrogen evolution. The photocatalytic activity was investigated under effective 100 $mWcm^{-2}$ of UV-Vis irradiation from a 300 W Xe lamp. The evolution of hydrogen gas was then detected through headspace gas analysis with a gas chromatograph (Agilent 7890B) equipped with a HP-MOLESIEVE column and a thermal conductivity detector (TCD) with argon as the carrier gas. A 1 mL sample volume was extracted from the reactor headspace at 1 hr interval by using a gas tight syringe with valve. The integrated peak area was converted into the amount of hydrogen production by comparison of the peak area of a standard hydrogen curve.

Reference

1 H. Ataee-Esfahani, L. Wang, Y. Nemoto and Y. Yamauchi, *Chem. Mater.*, 2010, **22**, 6310–6318.

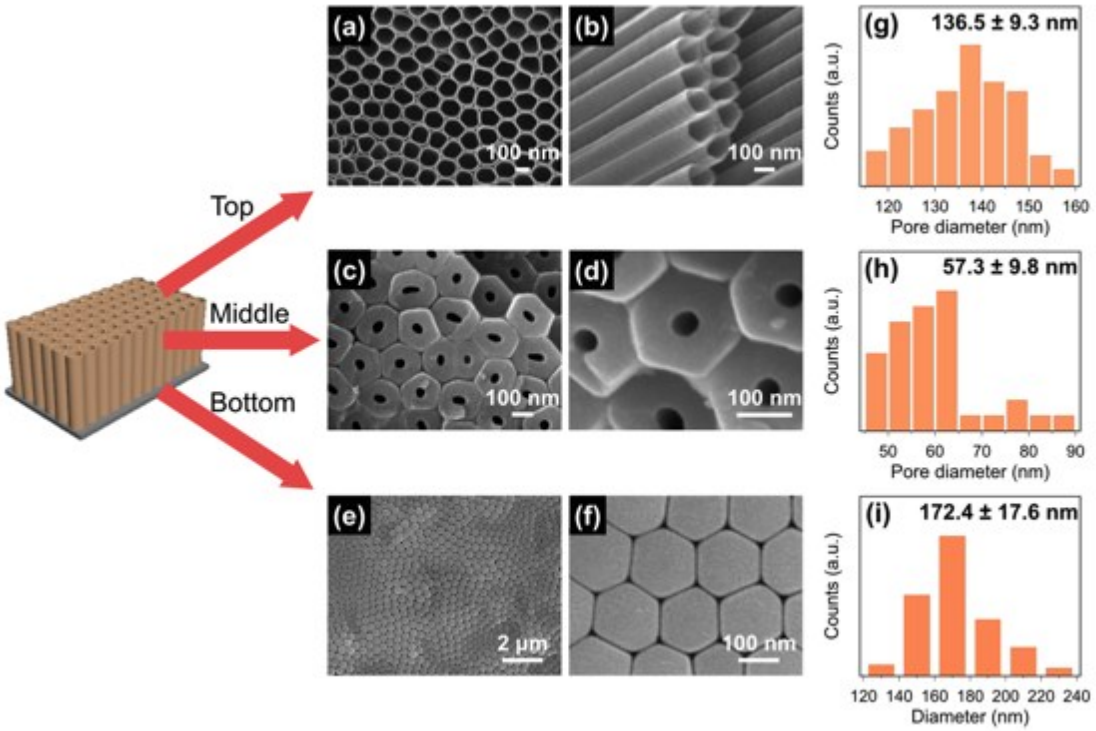

Fig. S1 SEM images and diameter analysis of TiO_2 nanotubes with different regions. (a) and (b) the top view, (c) and (d) the middle region, (e) and (f) the bottom region of TiO_2 nanotubes. The top-view of the thin film showed that uniform tubes were formed during anodization and the inner-diameter of nanotube wasaround 100 nm, which would provide sufficient space to deposit Au@Pt nanostructure. The inner-diameter was diminished to only 50 nm at the middle of the nanotube and eventually reached to closed end at the bottom of the nanotube. The unique "V" shape cross-section of nanotube was detrimental to the self-assembling of Au@Pt nanostructure on the surface of TiO_2 NTs, so that we scraped TiO_2 NTs with uniform tube diameter for further utilization. (g) and (h) the statistics of pore diameter of top part and middle part, respectively. (i) the statistics of cap diameter because no pore was shown at bottom.

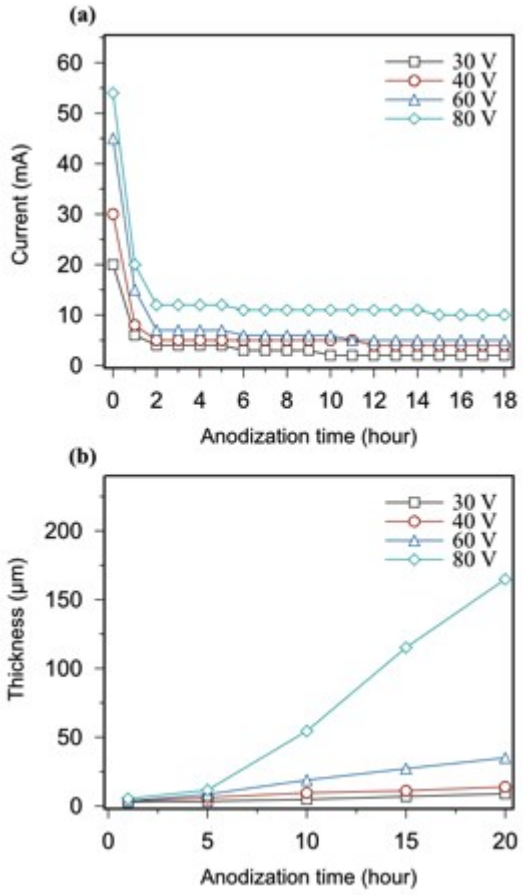

Fig. S2 (a) Corresponding current in various applied voltages during the anodization. High current appeared at the initial stage because large amount of Ti^{4+} ions were released from Ti foil into the electrolyte. Meanwhile, Ti^{4+} ions rapidly reacted with water to form dense TiO_2 thin film on the surface of Ti foil, so that the current gradually decreasedwith time. Subsequently, stable current was observed at later period as the etching rate achieved stable and steady. (b) The film thickness at various anodization time. Generally speaking, the thickness of TiO_2 NTs could be uniformly grown after five hours of anodization time. Too long of the growth time could make the TiO_2 NTs more defects, which deteriorated the charge transportation while tube shape of TiO_2 could not be formed at short growth time. Therefore, moderate growth time 15 hours at 60 V bias of anodization was chosen as typical condition in this work.

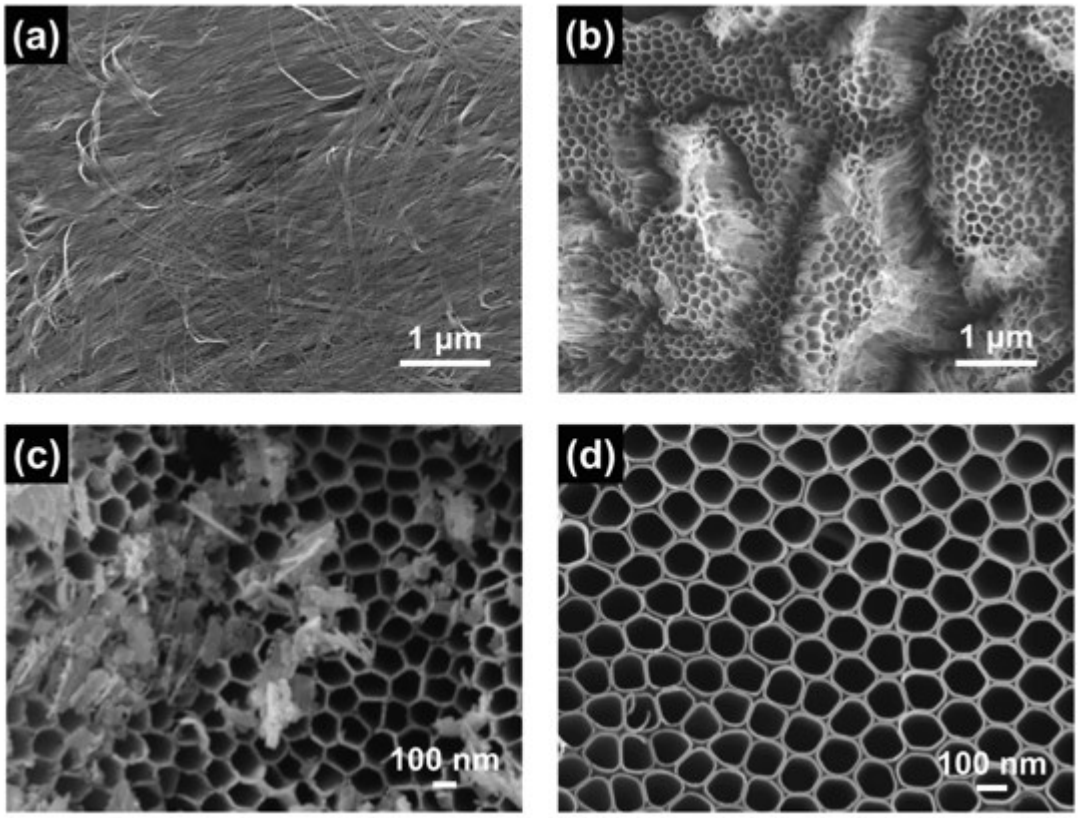

Fig. S3 SEM images of TiO_2 nanotubes with various ultrasonication time: (a) without ultrasonication, (b) 20 seconds, (c) 40 seconds, and (d) 60 seconds. After anodization, silk-like TiO_2covered on the top of the as-prepared TiO_2 nanotubes. Ultrasonication of 1 min was necessary to remove this silk-like TiO_2 completely. Over-time ultrasonication would result in the defects formation or collapse of the nanotubes.

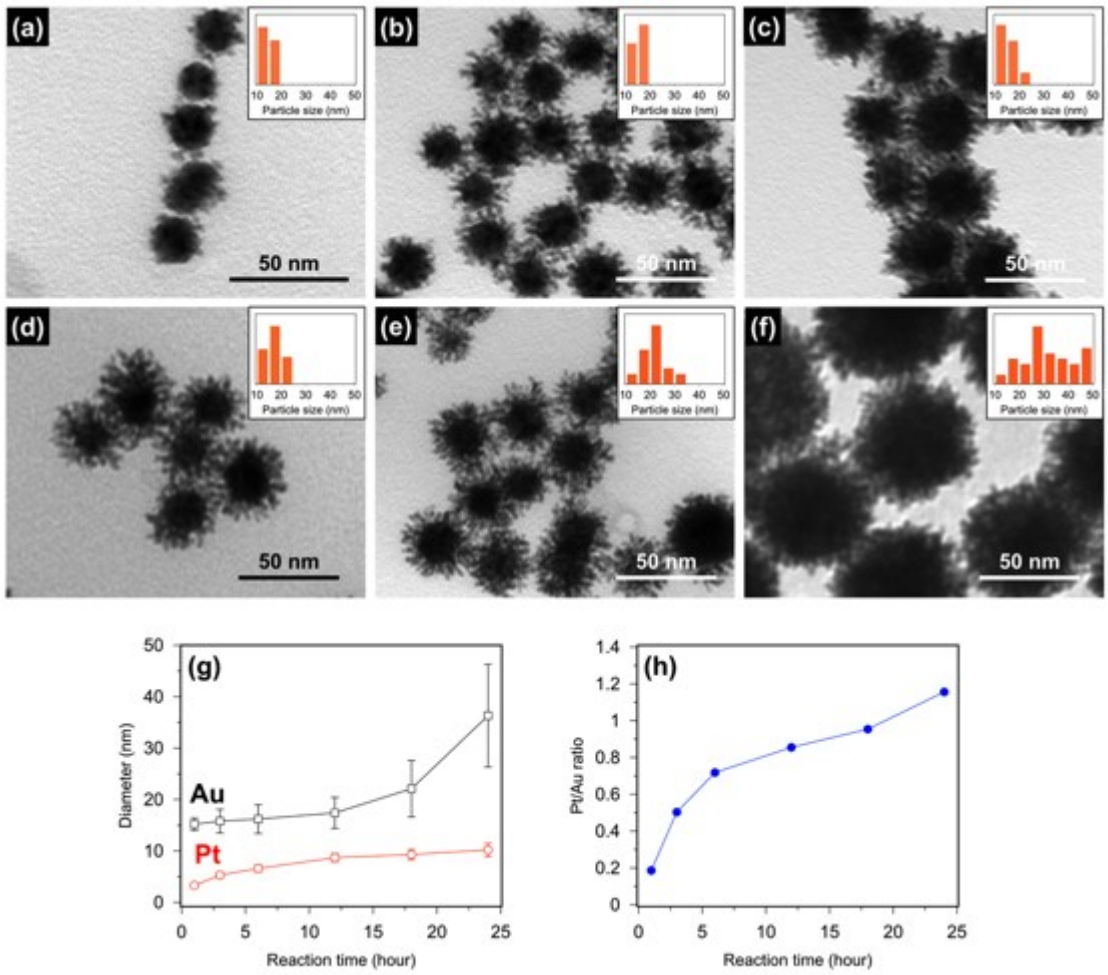

Fig. S4 TEM images and size statistics (the inset) of Au@Pt nanostructures: (a) 1 hr, (b) 3 hrs, (c) 6 hrs, (d) 12 hrs, (e) 18 hrs, and (f) 24 hrs. (g) The individual size of Au and Pt. Au-core had the nearly identical size until 16 hours of reaction time, but it would become much larger and less uniform with longer reaction time. On the other hand, Pt-shell grew thicker at the initial time, and then it remained almost the same thickness but had the more densed porous structure at longer reaction time. (h) The composition analysis of Au@Pt nanostructure. The Pt/Au ratio was much lower than one at the initial time, indicative of the mechanism that gold would nucleate first and grow as the particles, and subsequently platinum deposited on the gold surface. The ratio of Pt/Au nanostructurebecame higher when the reaction continued and eventuallyreached over one at 24 hours of reaction time.

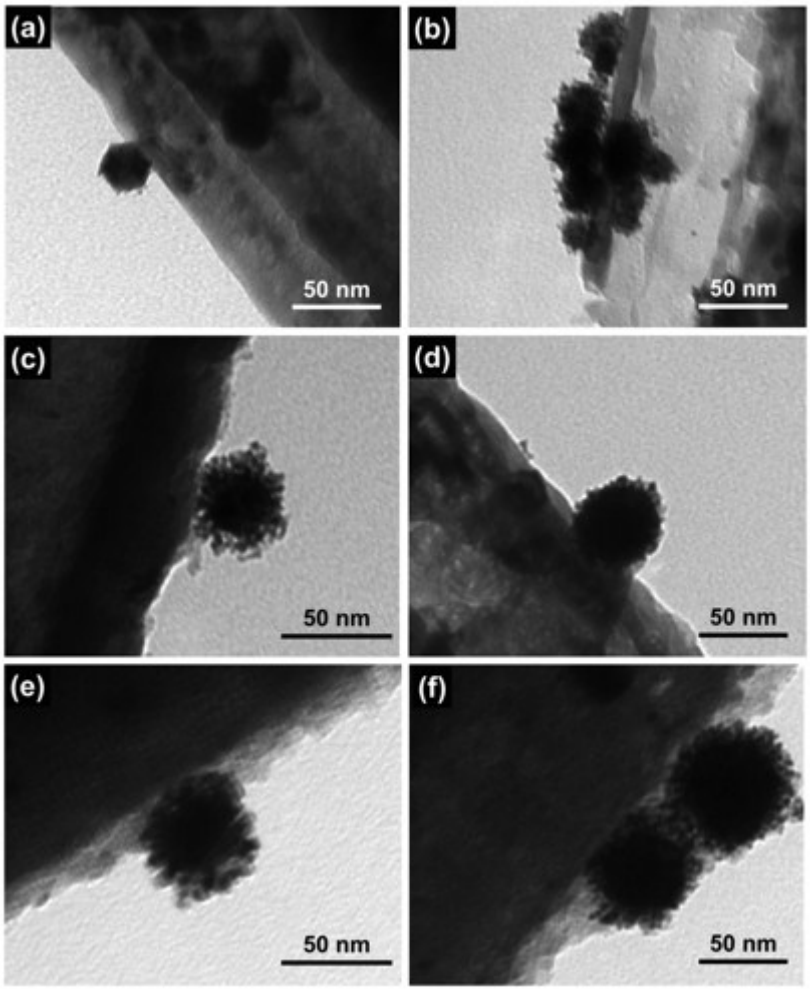

Fig. S5 TEM images of TiO_2 NTs-Au@Pt composite with various conditions of Au@Pt nanostructure: (a) 1 hr, (b) 3 hrs, (c) 6 hrs, (d) 12 hrs, (e) 18 hrs, (f) 24 hrs. With surface modification of 3-MPA on Au@Pt nanostructure, Au@Pt nanostructure could successfully self-assembled on the surface of TiO_2 NTs. Au@Pt nanostructure did not change its morphology during self-assembling in all conditions.

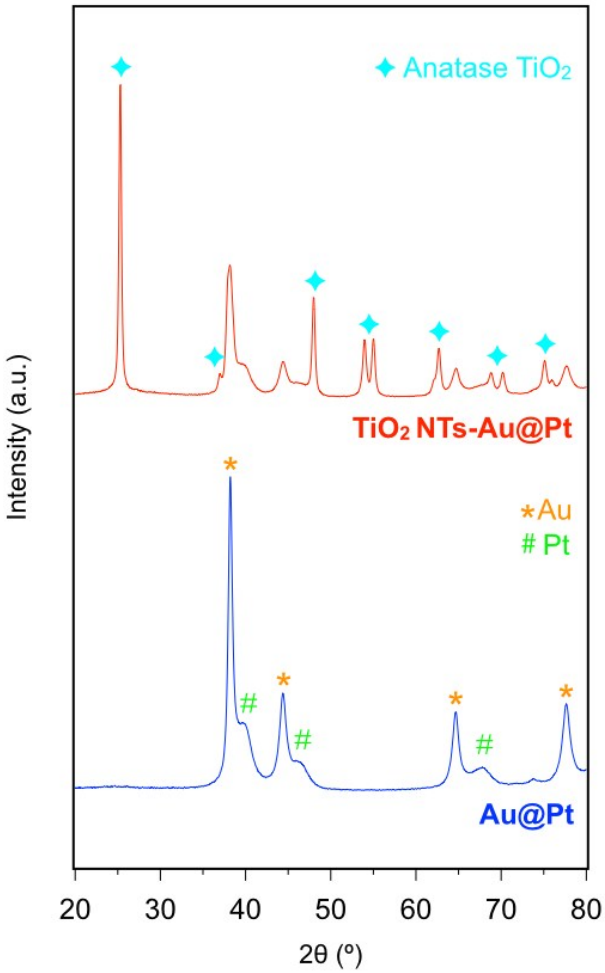

Fig. S6 X-ray diffraction patterns of Au@Pt, and TiO_2 NTs-Au@Pt samples.In the XRD pattern of Au@Pt, the diffraction peaks showed distinct feathers of Au and Pt. Moreover, Au with narrow peak width and Pt with broad width, which corresponded with the observed size distribution of individual metals. The self-assembled TiO_2 NTs-Au@Pt composite presented the crystalline combination of TiO_2 NTs and Au@Pt nanostructure without peak shift and destructive diffraction.

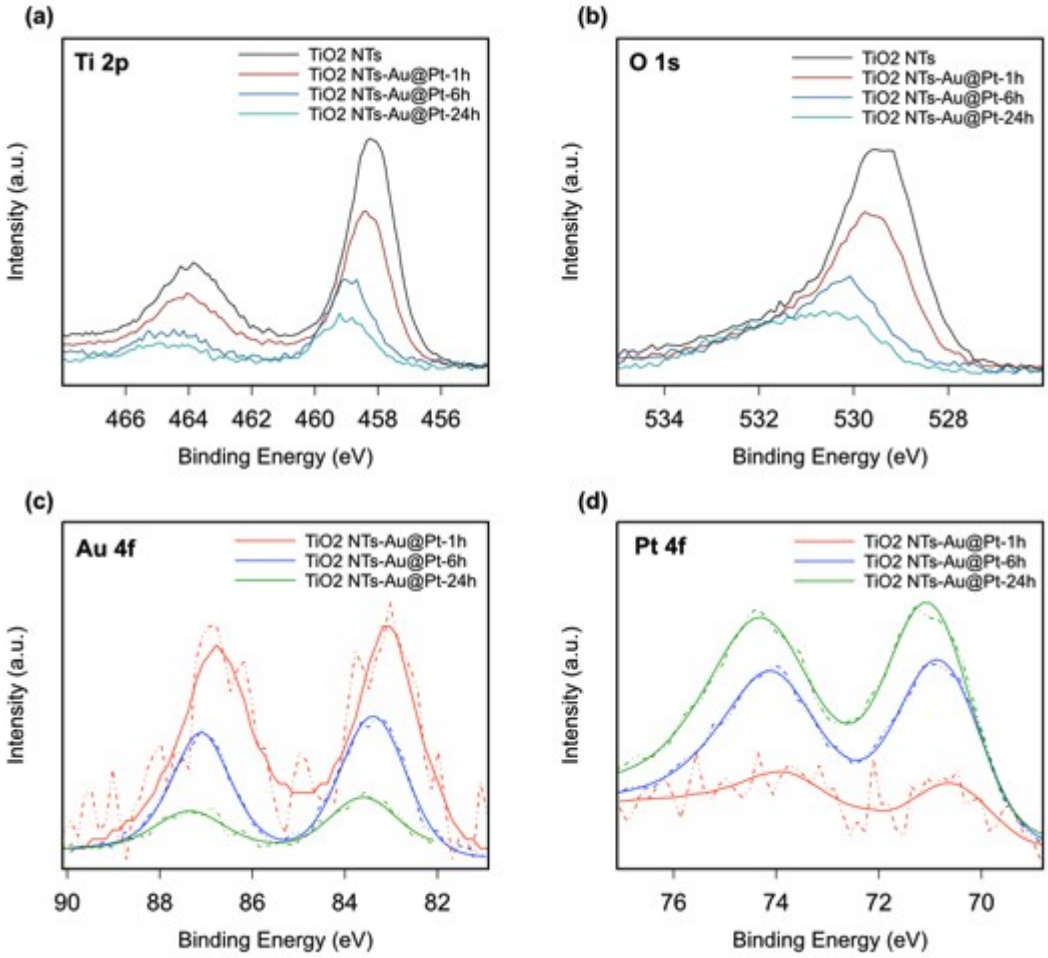

Fig. S7 XPS spectra for TiO_2NTs-Au@Pt composite: (a) Ti 2p and (b) O 1s. The binding energy of Ti 2p suggested the typical anatase phase of TiO_2 NTs.(c) Au 4f, and (d) Pt 4f of TiO_2 NTs-Au@Pt composite. The peak position of Au and Pt vastly shifted with increased platinum content.In (c) and (d), Dash lines represent the experimental data while solid lines are the fitting results.

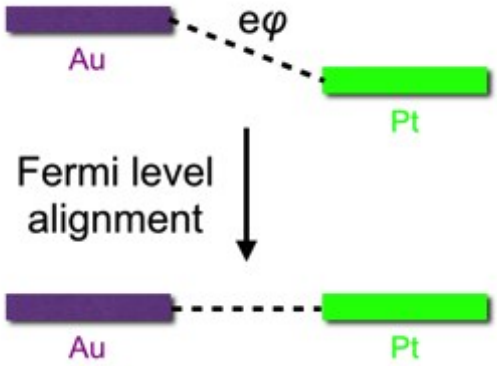

Fig. S8 The schematic illustration of an extra electric field induced by well-defined Au@Pt during Fermi level alignment

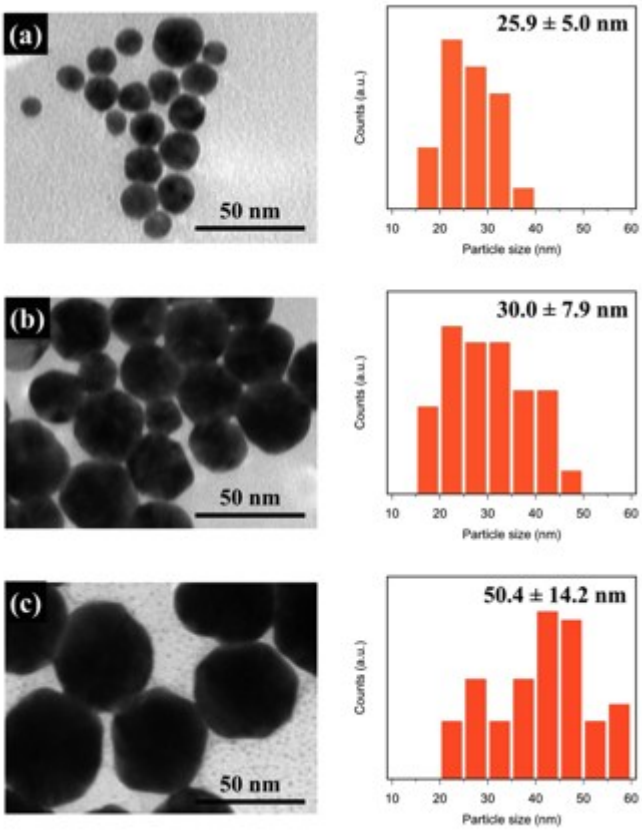

Fig. S9 TEM images of Au nanoparticles with different reaction time without addition of H_2PtCl_6at the synthesis: (a) 1 hr, (b) 6 hrs, and (c) 24 hrs. Au nanoparticle exhibited spherical shape. The size statistics of Au nanoparticles matched that of Au core in Au@Pt nanostructure.

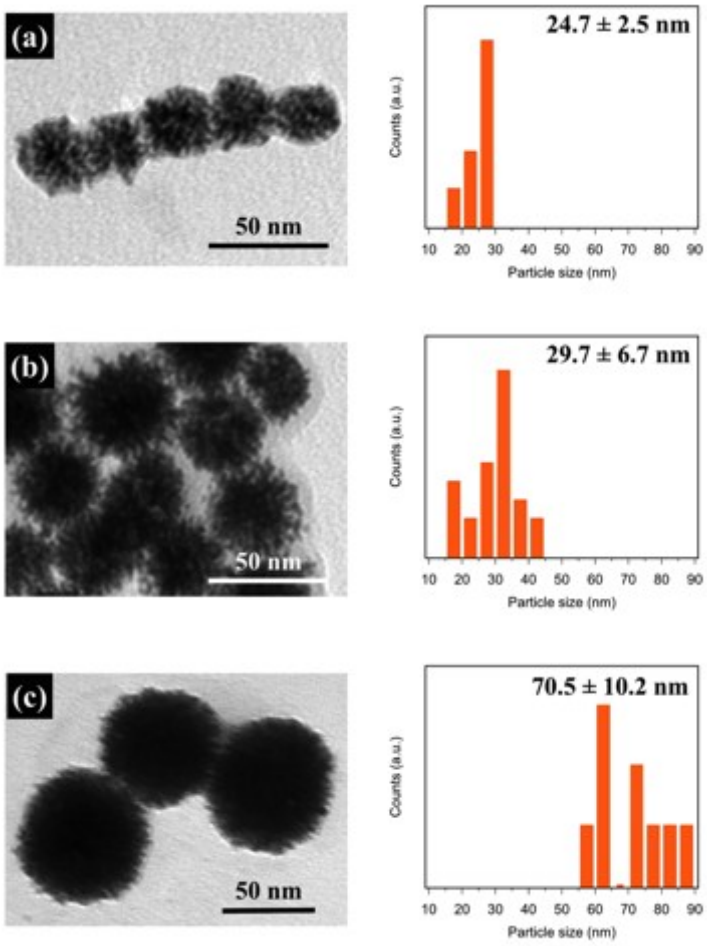

Fig. S10 TEM images of Pt clusters with different reaction time without addition of $HAuCl_4$ at the synthesis: (a) 1 h, (b) 6 hrs, and (c) 24 hrs. The size statistics of Pt clusters showed that the amount of Pt could increase with the longer growth time, corresponding with the increase amount of Pt shell in Au@Pt nanostructure.

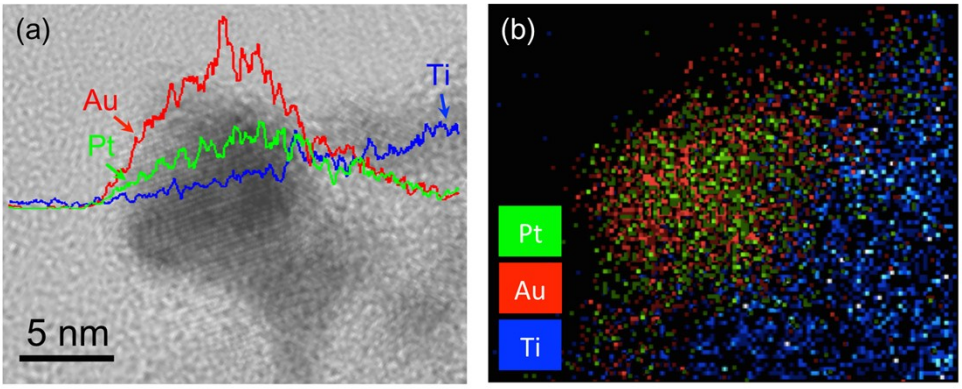

Fig. S11 Microstructure of TiO_2 NTs-AuPt photocatalyst and the elemental analysis: (a) HR-TEM combined with EDX line scans of Ti, Au, and Pt. (b) STEM image hybrid with EDX mapping. All the elemental analysis suggested that Au and Pt were formed as a random alloy in the nanoparticle.

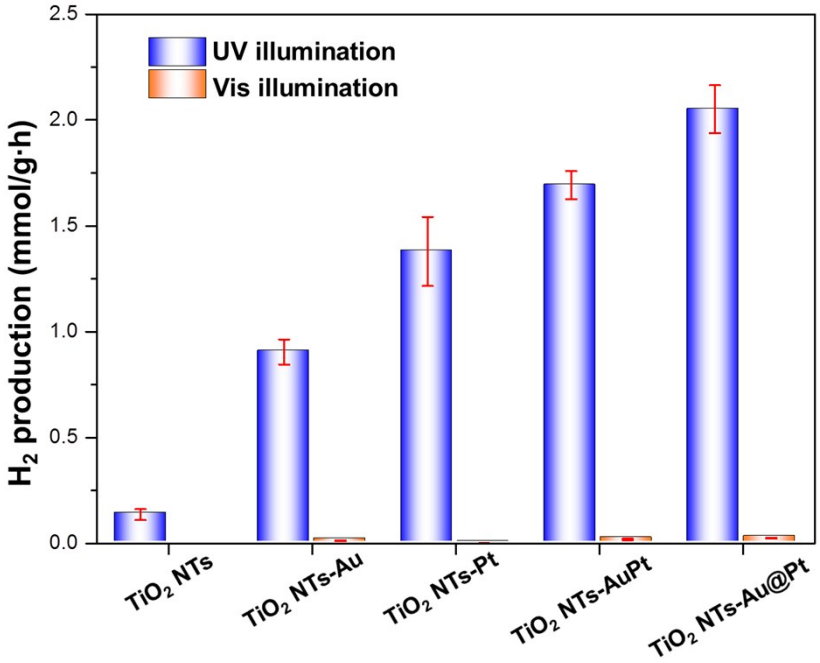

Fig. S12 H_2 evolution of TiO_2 NTs, TiO_2 NTs-Au, TiO_2 NTs-Pt, TiO_2 NTs-AuPt, and TiO_2 NTs-Au@Pt samples in UV or visible regions.

In order to specify the LSPR effects for hydrogen production, the 450 nm long pass filter was utilized to reveal the photocatalytic activities in visible region. In this test, we detected only trace amount of hydrogen gases in each catalyst, e.g. TiO_2 NTs, TiO_2 NTs-Au, TiO_2 NTs-Pt, TiO_2 NTs-AuPt, and TiO_2 NTs-Au@Pt (as shown in Fig. S12). Owing to the fact that absence of light absorption in TiO_2 NTs, the hydrogen generation in visible region should be attributed to the hot electron excited in Au by SPR effect. In order to verify the hydrogen generation in UV region, the UV pass filter was employed to reveal the photocatalytic properties of UV range and the results were also showed in Fig. S12. Noted that the hydrogen generation in visible region was much lower than that in UV region and white light (shown in Fig. 3c), it suggested that the significant enhancement of hydrogen production as a result of hot electrons excited in Au by SPR effect could be ruled out and also confirmed that the

enhancement could be attributed to the synergistic effects owing to downshifted Schottky barrier between TiO_2 NTs and metals as well as plasmon-induced resonance energy transfer (PIRET) effect. The results of hydrogen production of all samples in UV region were slightly lower than those corresponding performance in UV-vis region (white light), which meant that co-catalysts decoration could significantly improve the charge separation to enhance their photocatalytic hydrogen generation since both Pt and Au nanostructures were unable to contribute any significant electrons to photocatalytic hydrogen generation (Fig. S12). All photoelectrons utilized to generate hydrogen gas could be attributed to the photoexcitation of TiO_2 rather than any photoexcitation of metallic nanostructure, indicated that the photocatalytic performance of each sample was strongly dependent on the charge-separation of photoinduced electrons upon TiO_2. Notably, to consider the enhanced ratio of the UV light illumination to UV-vis light illumination, the TiO_2 NTs-Au sample (1.43/0.9) performed a larger enhancement than that of TiO_2 NTs-Pt sample (1.67/1.38), suggested that SPR effect could provide additional efforts to hydrogen generation while the photocatalytic performance of TiO_2 NTs-Au sample was still lower than that of TiO_2 NTs-Pt sample. As a result, we could expect that bimetallic AuPt nanostructures with both random alloy and core-shell forms could exhibit better activities than that of single element nanostructure. Furthermore, the TiO_2 NTs-Au@Pt sample could significantly show a better enhancement of photocatalytic activity (2.97/2.05) than that of TiO_2 NTs-AuPt alloy sample (2.18/1.69), which also suggested that core-shell nanostructure was able to offer additional effects for enhancing their charge-separation and photocatalytic activity. Consequently, we could

conclude that a synergistic effect from core-shell nanostructure allowed us to facilitate the charge-separation and maximize the corresponding photocatalytic performance of semiconductors.

Table S1 Summary of elemental analysis of TiO_2 NTs-Au@Pt composite, the hydrogen production and the normalized hydrogen production. Owing to the variation amount of catalyst (Au and Pt) on different TiO_2 NTs-Au@Pt composites, the normalized hydrogen production was calculated by dividing the weight of TiO_2 NTs, which was measured by ICP-Mass.

		TiO_2 NTs-Au@Pt-1h	TiO_2 NTs-Au@Pt-3h	TiO_2 NTs-Au@Pt-6h	TiO_2 NTs-Au@Pt-12h	TiO_2 NTs-Au@Pt-18h	TiO_2 NTs-Au@Pt-24h
Composition (atomic%)	Ti	86.09	78.99	84.54	83.32	84.95	83.65
	Au	11.61	16.49	12.25	11.94	10.10	10.94
	Pt	2.30	4.51	3.22	4.74	4.96	5.41
Catalyst Weight (mg)	TiO_2	3.58	3.02	3.45	3.35	3.48	3.38
	Au	1.19	1.56	1.23	1.18	1.02	1.09
	Pt	0.23	0.42	0.32	0.47	0.50	0.53
H_2 production ($\mu molg^{-1}h^{-1}$)		288 ± 36	543 ± 34	2971 ± 174	1620 ± 100	488 ± 33	253 ± 12
H_2 production ($\mu molg_{TiO_2}^{-1}h^{-1}$)		402 ± 60	899 ± 56	4306 ± 252	2418 ± 149	701 ± 47	374 ± 18